Investigations on the role of impaired lysosomes of macrophages in disease

Lienden, M.J.C. van der

Chapter 5

GCase and LIMP2 abnormalities in the liver of Niemann Pick type C mice

Contributing authors:

M.J.C. van der Lienden, M. van Eijk, J. Aten & J.M.F.G. Aerts. *To be submitted.*

Abstract

The lysosomal storage disease Niemann Pick type C (NPC) is caused by impaired cholesterol efflux from lysosomes which is accompanied by secondary lysosomal accumulation of sphingomyelin and glucosylceramide (GlcCer). Similar to Gaucher disease (GD) patients deficient in glucocerebrosidase (GCase) degrading GlcCer, NPC patients show an elevation in glucosylsphingosine and glucosylated cholesterol. In livers of mice lacking the lysosomal cholesterol efflux transporter NPC1, we investigated the expression of established biomarkers of lipid-laden macrophages in GD patients, their GCase status, and the presence of the cytosol facing glucosylceramidase GBA2 and LIMP2, the transporter of newly formed GCase to lysosomes. Livers of 80-week-old *Npc1*$^{-/-}$ mice showed a partial reduction in level of GCase protein and enzymatic activity. In contrast, GBA2 levels tended to be reciprocally increased compared to GCase deficiency. In *Npc1*$^{-/-}$ liver, increased expression of lysosomal enzymes (cathepsin D, acid ceramidase) was observed as well as an increase in markers of lipid-stressed macrophages (GPNMB and galectin-3). Immunohistochemistry showed that the latter markers are expressed by lipid laden Kupffer cells. An elevation of LIMP2 in *Npc1*$^{-/-}$ liver was detected by western blotting. Unexpectedly, immunohistochemistry revealed a marked overexpression of LIMP2 specifically in hepatocytes of the *Npc1*$^{-/-}$ liver. The subcellular distribution of LIMP2 and LAMP1 in NPC1-deficient hepatocytes differed, suggesting that LIMP2 not only localizes to (endo)lysosomes. The recent recognition that LIMP2 harbours a cholesterol channel prompts the speculation that LIMP2 in *Npc1*$^{-/-}$ hepatocytes mediates export of cholesterol into the bile and thus protects the hepatocytes.

Introduction

The liver plays a key role in maintaining bodily cholesterol homeostasis. It produces, metabolizes, secretes, and endocytoses cholesterol. Following the endocytic uptake by hepatocytes and Kupffer cells, cholesterol is exported from their (endo)lysosomes to the cytosol. This process is carried out by the lysosomal proteins NPC1 and NPC2.[1] The latter protein transfers cholesterol from (endo)lysosomal luminal membrane vesicles to the lysosomal membrane protein NPC1 that next mediates its efflux from the lysosome. Deficiencies in either NPC1 or NPC2 cause Niemann Pick disease type C (NPC), a lysosomal storage disorder characterized by lysosomal accumulation of cholesterol that is accompanied by increases in other lipids including sphingomyelin and glucosylceramide (GlcCer).[2] In NPC liver, lysosomal lipid accumulation is more prominent in Kupffer cells than hepatocytes.[3]

The secondary accumulation of GlcCer in NPC liver suggests interaction between cholesterol and GlcCer metabolism. Several other findings point to this. For example, the activity of glucocerebrosidase (GCase), the lysosomal β-glucosidase degrading GlcCer to ceramide, is found to be reduced in NPC.[4–6] Indeed, like GCase-deficient GD patients, NPC patients show an elevation in glucosylsphingosine (GlcSph).[7] GlcSph is also increased in tissues and plasma of *Npc1*$^{-/-}$ mice. GlcSph is formed from excessive lysosomal GlcCer by acid ceramidase.[8] GCase is also known to act as transglucosidase, generating glucosylated cholesterol (GlcChol) during lysosomal cholesterol accumulation.[9] Consequently, GlcChol is more than fifty-fold elevated in liver of *Npc1*$^{-/-}$ mice and significantly increased in plasma of NPC1-deficient mice and patients.[9] Under normal conditions, GlcChol is synthesized by the cytosol-facing enzyme GBA2 and is degraded to glucose and cholesterol by GCase in lysosomes.[10]

The enzyme GCase is transported to lysosomes being bound to the membrane protein LIMP2.[11] Following folding in the endoplasmic reticulum, GCase associates to LIMP2 and the complex is routed to lysosomes were dissociation is favored by the locally low pH.[12,13] Recently it has become apparent that LIMP2 contains a putative channel allowing transport of cholesterol molecules.[14] During deficiency of NPC1, LIMP2 appears to be involved in cholesterol efflux from lysosomes.[14] This is substantiated by the observation that a dual deficiency in NPC1 and LIMP2 results in a more prominent SREBP2-driven induction of HMGCoA reductase transcription, a classic readout for impaired cholesterol efflux from lysosomes.[14] Of note, LIMP2-deficient mice show no marked abnormalities in cholesterol homeostasis, suggesting that NPC1 is normally sufficient to govern cholesterol efflux from lysosomes.[9]

A striking similarity between NPC and GCase-deficiency (GD) is the overexpression of specific proteins by lipid-laden macrophages. In GD, GlcCer-laden macrophages excessively produce the chitinase chitotriosidase, the chemokine CCL18 and GPNMB.[15–19] In plasma of symptomatic Gaucher patients, chitotriosidase, CCL18 and a soluble fragment of GPNMB are spectacularly increased and these abnormalities are exploited as biomarkers.[20] Increased plasma levels of these biomarkers also occur in NPC.[21,22] Finally, increased metabolism of GlcCer by the cytosol-facing glucosylceramidase GBA2, which is observed during GCase deficiency, has also been noted in brain of *Npc1*$^{-/-}$ mice.[10] Pharmacological inhibition of GBA2 activity with a hydrophobic iminosugar, or GBA2 gene ablation, remarkably ameliorates neuropathology in *Npc1*$^{-/-}$ mice and increases their

life span.[10,23]

We examined the status of GCase in the liver of mice lacking the NPC1 protein and determined the expression of biomarkers of lipid-laden macrophages. Furthermore, we investigated the status of GBA2 and LIMP2. Our study revealed an expected increased expression of biomarkers of lipid-stressed macrophages, but it also disclosed remarkable upregulation of LIMP2 in hepatocytes.

Results

Structural analysis of Npc1$^{-/-}$ liver

The livers of 80-days-old *Npc1$^{-/-}$* mice showed clusters of enlarged macrophages as visualized by toluidine blue staining (**Figure 1A**). Ultrastructural analysis of the tissue by transmission electron microscopy (TEM) confirmed the presence in *Npc1$^{-/-}$* liver of characteristic, vacuole containing storage cells of macrophage origin (**Figure 1B**). Altered ultrastructure was also observed in the case of hepatocytes in the *Npc1$^{-/-}$* liver (**Figure 1B**). Of note, the *Npc1$^{-/-}$* hepatocytes contained clefts suggestive for deposition of cholesterol crystals (**Figure 1A & B**).[24–26]

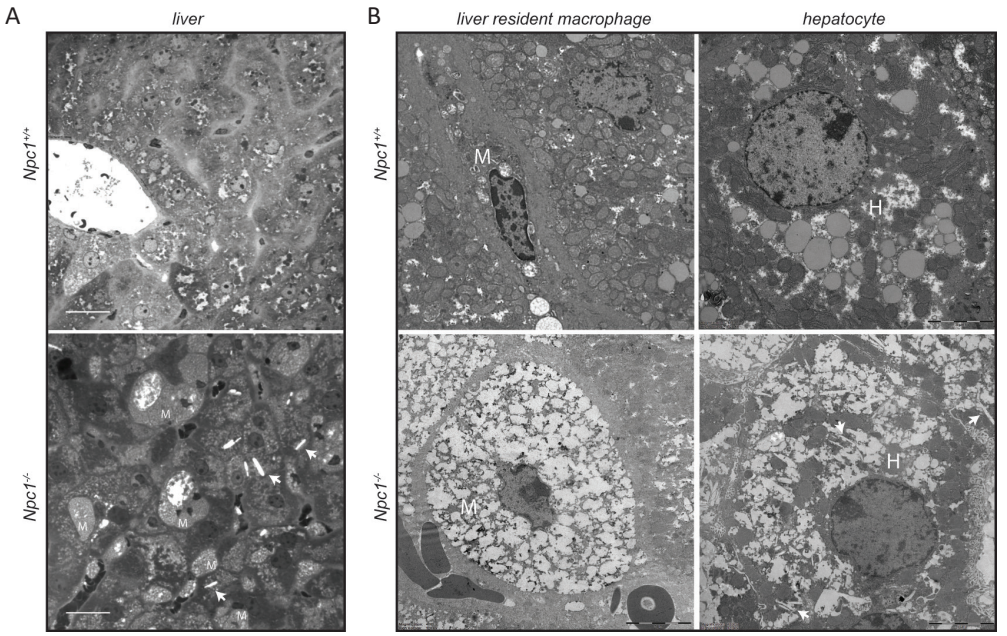

Figure 1. Structural analysis of liver of 80-days-old Npc1$^{+/+}$ and Npc1$^{-/-}$ mice. *(**A**) Micrographs of toluidine blue-stained sections. Scale bar=25μm; M: liver resident macrophage(clusters). (**B**) Transmission electron microscopy (TEM) micrographs of liver resident macrophages (M) and hepatocytes (H). Scale bar=5μm. Arrows indicate clefts in hepatocytes of NPC1$^{-/-}$ liver.*

Lysosomal GCase and cytosol facing GBA2 in Npc1$^{-/-}$ liver

The enzymatic activity of GCase in total *Npc1$^{-/-}$* liver extract was on average 60% reduced (**Figure 2A**). This reduction is similar to earlier observations made with Npc1$^{-/-}$ brain.[10] Of note, the expression of the *Gba1* gene tended to be upregulated in the *Npc1$^{-/-}$* liver (**Figure 2B**), which indicates that GCase in the *Npc1$^{-/-}$* liver is post-transcriptionally

reduced. An activity-based probe, covalently binding to the catalytic nucleophile of retaining β-glucosidases, was used to simultaneously visualize active GCase (59-66 kDa) and GBA2 (110 kDa) enzyme molecules in extracts of the various livers. Although considerable interindividual variation was noted for levels of GCase and GBA2 activities in livers (**Figure 2C**), a reduction in GCase was found to correlate with an elevation of GBA2 (**Figure 2D**).

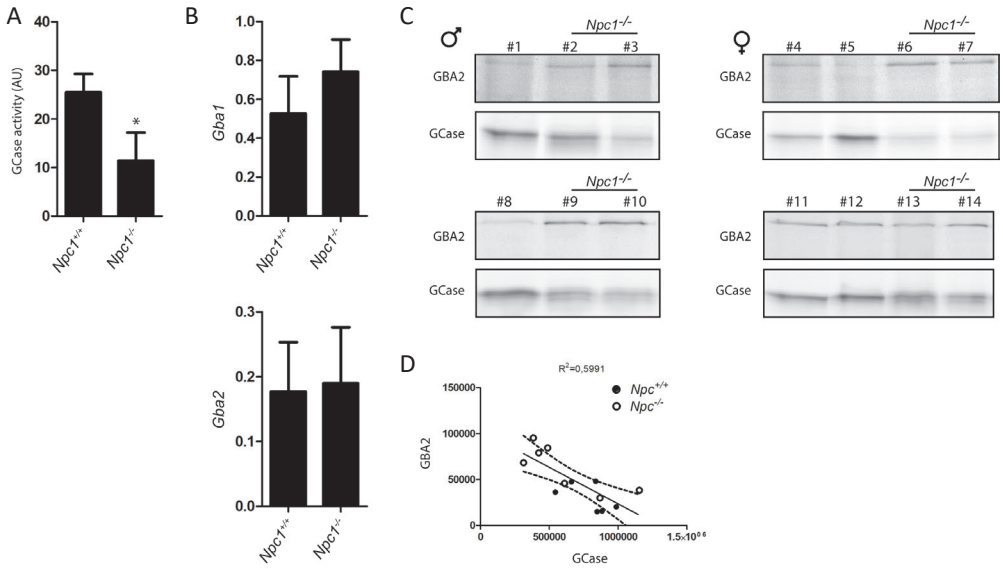

Figure 2. Lysosomal GCase and cytosol facing GBA2 in NPC$^{+/+}$- and Npc1$^{-/-}$ mouse liver. *(**A**) GCase activity was measured in liver lysates of NPC1$^{+/+}$- and NPC$^{-/-}$-mice with 4MU-β-Glc substrate as described in M&M. (**B**) Real-time (Rt) qPCR RNA analysis on Gba1 and Gba2 gene expression in lysates of the same livers. Values represent relative numbers compared to ribosomal gene Rplpo. (**C**) GCase and GBA2 in aliquots of the same lysates were labelled with GCase-specific ABP and subsequently visualized by fluorescence scanning after SDS-PAGE. # Npc1$^{+/+}$: 1, 4, 5, 8, 11, 12; # Npc$^{-/-}$: 2, 3, 6, 7, 9, 10, 13, 14. (**D**) Reciprocal correlation between overall active GCase and GBA2 molecules in liver lysates of Npc1$^{+/+}$- and Npc1$^{-/-}$ mice based on quantification of labelled bands in C.*

Response to lysosomal storage in NPC liver

Npc1$^{-/-}$ mice exhibit a striking degree of storage that is particularly confined to macrophages. Lysosome perturbation by storage is usually accompanied by increased lysosomal biogenesis and expression of particular markers such as GPNMB.[22,27] Employing western blotting, a clear increase in GPNMB in *Npc1$^{-/-}$* livers was demonstrable (**Figure 3A**). Likewise, the lysosomal membrane protein LAMP1 and galectin-3, a protein associated with lysosome stress, were found to be increased as visualized by western blotting. Next, the expression of illustrative genes encoding lysosomal proteins was analysed (**Figure 3B**). We noted markedly increased expression of the *Gpnmb* and *Lgals3* genes, coding for GPNMB and galectin-3. No significant upregulation of expression of the genes *Lamp1*, encoding the lysosomal membrane protein LAMP1 and *Atp6v1a*, encoding the ATPase H^+ transporting V1 subunit A, was detected. However, an increased expression of *Asah1*, encoding acid ceramidase, and *Ctsd*, encoding cathepsin D was observed in the

NPC1-deficient mouse livers. Furthermore, the *Npc1*$^{-/-}$ mouse livers showed increased expression of genes coding for proteins implicated in inflammation (TNFα, CCL2; **Figure 3C**). No clear changes were observed in expression of the *Iba1* gene, which encodes for a commonly used marker of macrophages (**Figure 3C**).

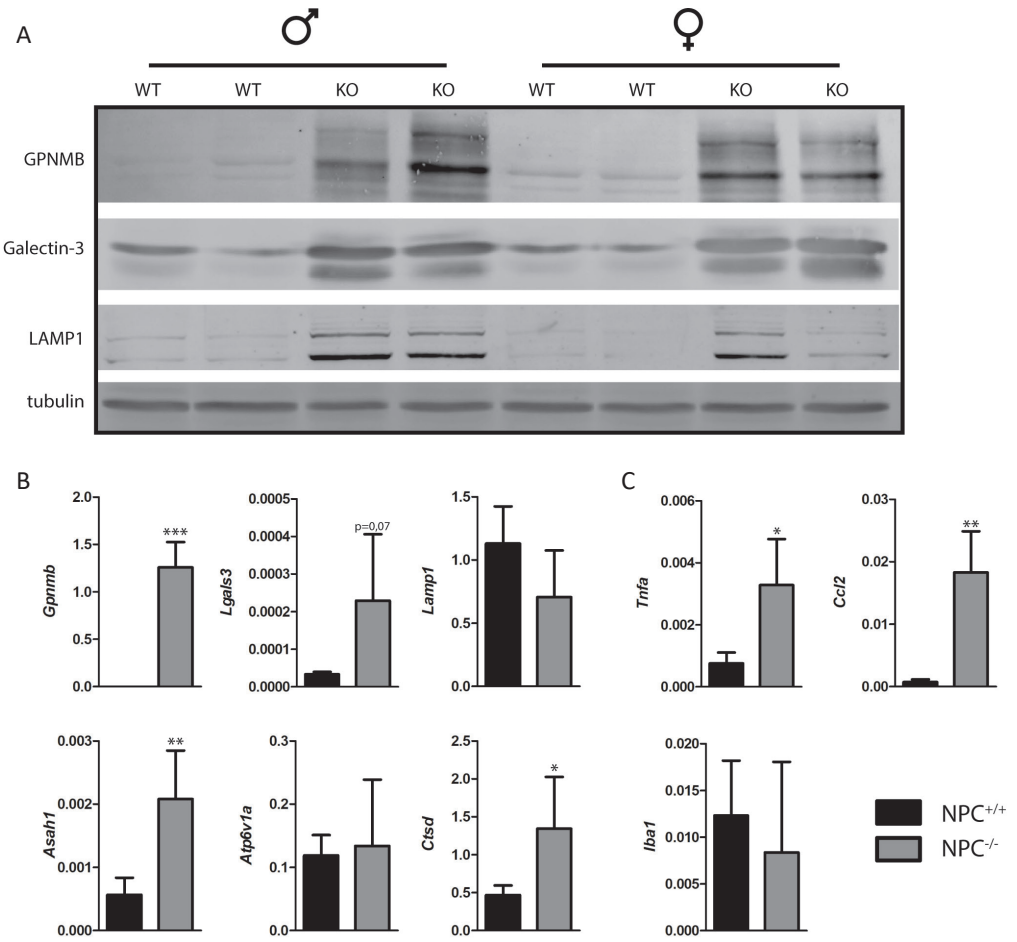

Figure 3. Response to lysosomal storage in NPC liver. *(**A**) Western blot analysis of lysosome storage associated proteins in lysates of Npc1*$^{+/+}$*- and Npc1*$^{-/-}$ *mouse liver; Real-time (Rt) qPCR RNA analysis of the same livers regarding lysosomal storage associated genes (**B**) and inflammatory genes (**C**). Values represent relative numbers compared to ribosomal gene Rplpo.*

LIMP2 upregulation in Npc1$^{-/-}$ *liver but not in cultured cells with pharmacologically induced lysosomal cholesterol accumulation*

Analysis of LIMP2 by Western blotting revealed a clear increase in the membrane protein in the *Npc1*$^{-/-}$ livers (**Figure 4A**). Next, we employed U18666A, an agent causing lysosomal cholesterol accumulation. No change in morphology was detected in HEPG2 cells treated with U18666A (**Figure 4B**). Treatment of HepG2 cells with U18666A caused a reduction in GCase as detected with activity-probe labelling but no change in LIMP2 as detected by western blotting (**Figure 4C**). In other words, the findings with NPC1-deficient liver for

LIMP2 were not recapitulated in cultured cells.

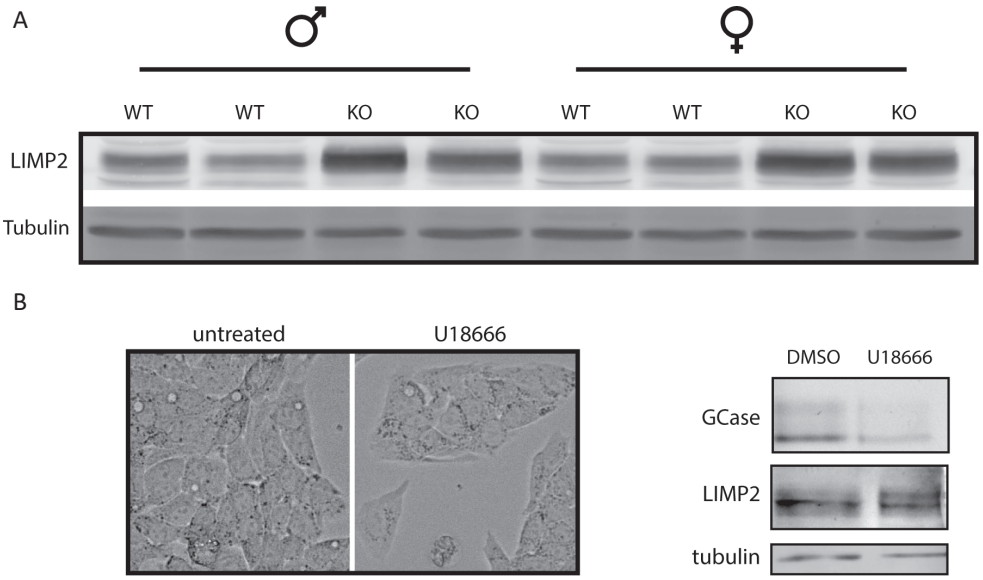

Figure 4. LIMP2 in NPC liver and U18666A treated HEPG2 cells. *(**A**) Western blot analysis of LIMP2/SCARB2 in lysates of Npc1$^{+/+}$- and Npc1$^{-/-}$ mouse liver. (**B**) Phase contrast microscopy pictures of HEPG2 cells treated with NPC1-inhibitor U18666A. (**C**) GCase (GBA) in HEPG2 lysates was labelled with GCase-specific ABP and subsequently visualized by fluorescence scanning after SDS-PAGE. LIMP2/SCARB2 was analysed by western blotting of the same wet gel slab as described in M&M.*

Immunohistochemical analysis of Npc1$^{-/-}$ liver

To visualize the cellular source of the excessive macrophage marker galectin-3 as well as that of the lysosomal protease cathepsin D and LIMP2 in liver of 80 days old *Npc1$^{-/-}$* mice, immunohistochemistry was applied. Contrary to matched control liver, the *Npc1$^{-/-}$* tissue showed the presence of lipid-laden macrophages (Kupffer cells, positive for Iba1), previously reported to markedly express GPNMB (**Figure 5A**).[22] Galectin-3 and cathepsin D staining were found to be also prominent for these storage cells (**Figure 5A and B**). Unexpectedly, the analysis of LIMP2 revealed predominant labelling of hepatocytes in the *Npc1$^{-/-}$* liver (**Figure 5A**). The location of LIMP2 in a peribiliary zone in wildtype hepatocytes was expanded to a more widespread peripheral distribution in *Npc1$^{-/-}$* hepatocytes (**Figure 5B**). The altered distribution of LIMP2 in *Npc1$^{-/-}$* liver was confirmed by fluorescence microscopy (**Figure 5C**). Again, LIMP2 staining was prominent in the hepatocytes. In contrast, GPNMB and galectin-3 staining was abundant in storage macrophages of the *Npc1$^{-/-}$* liver (**Figure 5C**). Of note, the staining pattern for LIMP2 in hepatocytes differed from that of LAMP1, an integral lysosomal membrane protein (**Figure 5C**).

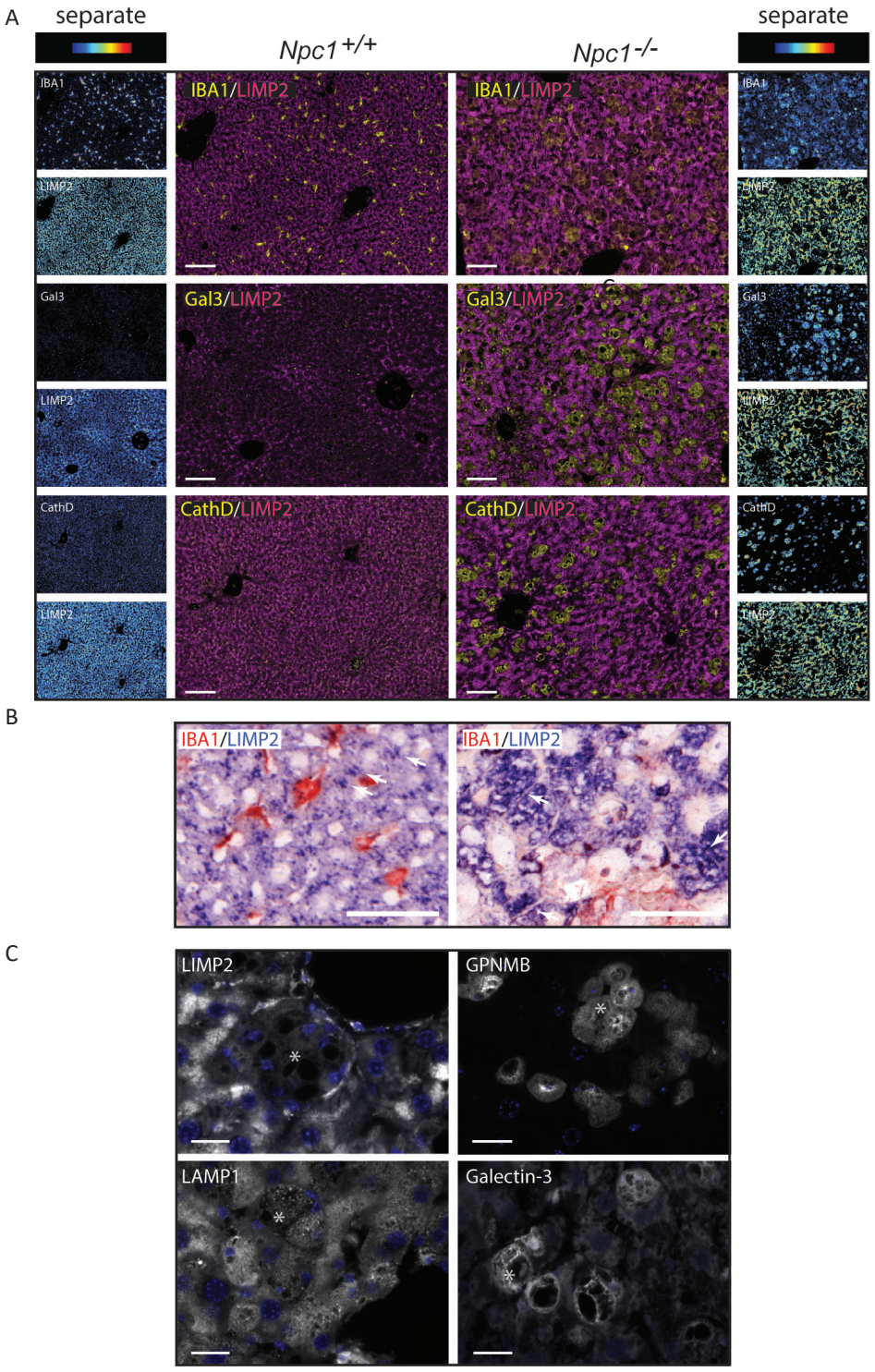

Figure 5. Immunohistochemistry *Npc1*$^{-/-}$ ***liver.*** *(**A**) 'Composite' panels of immunostaining of Npc1*$^{+/+}$*- and Npc1*$^{-/-}$ *liver of 80-days-old mice: LIMP2 is depicted in magenta and IBA1, galectin-3 and*

*cathepsin D in yellow. Brightfield scans were analysed using spectral imaging; separate images are displayed in heat-map intensity scale. Scale bar = 50 µm; (**B**) Higher magnification of livers from (A): LIMP2 is depicted in blue and IBA1 in red. Arrows indicate peribiliary LIMP2 localization in Npc1$^{+/+}$-hepatocytes and widespread location along apical and lateral membranes in Npc1$^{-/-}$ hepatocytes. Scale bar = 10 µm. (**C**) Immunofluorescence microscopy of the same livers (images taken with 63x magnification): LIMP2, GPNMB, LAMP1 and galectin-3. Nucleus is depicted in blue. Scale bar = 20 µm; asterisk indicates (clusters of) storage cells.*

Discussion

Our present study concerns abnormalities in GCase levels in the liver of mice that lack the lysosomal transmembrane protein NPC1 and consequently develop Niemann Pick disease type C. Earlier investigations already showed that the livers of *Npc1*$^{-/-}$ mice contain increased levels of GlcCer along with cholesterol.[7] In parallel, GlcSph is increased in the *Npc1*$^{-/-}$ liver. These studies indicate that local degradation of GlcCer by lysosomal GCase is impaired, which is followed by increased de-acylation through lysosomal acid ceramidase.[8] Moreover, livers of *Npc1*$^{-/-}$ mice accumulate GlcChol, which points to an increased transglucosylation activity of GCase.[9] Earlier work also described accumulation of GPNMB positive foamy cells in the liver of *Npc1*$^{-/-}$ mice, resembling Gaucher cells during a primary GCase deficiency (Gaucher disease).[22] We studied GCase in more detail in liver of *Npc1*$^{-/-}$ mice using activity-based probes that selectively label active enzyme molecules. In addition, we employed western blotting, qPCR and immunohistochemistry to examine other proteins known to be changed by GCase deficiency. ABP labelling confirmed reduction in active GCase content of liver of *Npc1*$^{-/-}$ mice. Reduction in GCase was accompanied by reciprocal increase of active GBA2 molecules in liver lysates of *Npc1*$^{-/-}$ mice. Of note, in brain of *Npc1*$^{-/-}$ mice, an increase in GBA2/GCase ratio was already observed previously[10] and genetic ablation or pharmacological inhibition of GBA2 in *Npc1*$^{-/-}$ mice significantly increases life span.[10] The reduction of GCase following lysosomal cholesterol accumulation was recapitulated *in vitro* with cultured HEPG2 cells treated with a known NPC1 inhibitor, U18666A. Our immunohistochemical investigation of liver of *Npc1*$^{-/-}$ mice confirmed the presence of characteristic storage cells that were positive for the macrophage marker Iba1. An increase in GPNMB in livers of 80 weeks old *Npc1*$^{-/-}$ mice was observed on RNA level, and by western blot. The foamy storage cells were found to overexpress GPNMB, galectin-3 and cathepsin D.

Immunohistochemical analysis of the NPC livers unexpectedly revealed a very prominent expression of LIMP2 in hepatocytes and not in the lipid-laden storage cells. The pattern of LIMP2 staining differed from that of lysosome marker LAMP1 regarding subcellular localization. Interestingly, inducing lysosomal cholesterol accumulation in HEPG2 cells with U18666A caused no overexpression of LIMP2. These findings show that cultured cells do not provide a phenocopy of the polarized hepatocytes in the *Npc1*$^{-/-}$ liver. The striking upregulation of LIMP2 in hepatocytes of the *Npc1*$^{-/-}$ liver and apparent partial non-lysosomal localization is intriguing and warrants further discussion. The morphology of NPC1-deficient hepatocytes is not considered to undergo prominent lysosomal storage associated changes.[3] It could be speculated that the upregulation of LIMP2 is instrumental to this. Heybrock et al. recently provided evidence that LIMP2 can assist efflux of cholesterol from lysosomes in an NPC1-independent manner. In NPC1-deficient cells, SREBP2 (Sterol regulatory element-binding protein 2) mediated transcription is

upregulated in response to the reduced cholesterol level in the endoplasmic reticulum that results from impaired sterol efflux from lysosomes. The transcription factor SREBP2 controls cholesterol homeostasis by stimulating transcription of genes encoding proteins involved in the biosynthesis of cholesterol.[28] A combined deficiency of NPC1 and LIMP2 was found to increase SREBP2-mediated *de novo* synthesis of cholesterol, which points to LIMP2-mediated cholesterol efflux from lysosomes during NPC1 deficiency.[14] Clearly, the efflux of cholesterol from lysosomes is primarily mediated by the NPC2/NPC1 pathway since individuals deficient in LIMP2 (ko mice and patients suffering from acute myoclonus renal failure syndrome, AMRF) show no signs of disturbed cholesterol metabolism.[29] If overexpression of LIMP2 serves as a compensatory mechanism to NPC1 deficiency, the question arises why such response does not seem to take place in the macrophage-like cells that transform into lipid storage macrophages. These cells seem to change instead by increasing storage capacity through upregulation of their lysosomes.

The apparent partial non-lysosomal location of LIMP2 in *Npc1*$^{-/-}$ hepatocytes prompts the hypothesis that LIMP2 could be additionally involved in the export of cholesterol to the bile. In view of this hypothesis, examination of *Npc1*$^{-/-}$ enterocytes may be of interest. It has been recognized for some time that cholesterol is exported from enterocytes into the intestinal lumen via so-called TICE (trans-intestinal cholesterol export).[30] Possibly, LIMP2 could also be a player in this physiologically relevant process of cholesterol export.

In conclusion, the present study on liver of *Npc1*$^{-/-}$ mice has led to the discovery of a prominent upregulation of LIMP2 in hepatocytes. These findings could give impetus to studies on compensatory mechanisms in lysosomal storage disorders and the beneficial value of these processes. Specifically, characterization of human NPC1-deficient liver and the putative role of LIMP2 in cholesterol efflux to the bile warrants further testing.

Materials & Methods

Cell Culture Experiments

RAW264.7 cells and HEPG2 cells (American Type Culture Collection, TIB-71 and HB-8065 resp.) were cultured in DMEM containing 10% fetal calf serum, 1% glutamax and 0,2% antibiotics (penicillin-streptomycin; all purchased from Thermo Fisher Scientific) at 37°C at 5% CO_2. NPC1 inhibition was performed using 10 µM U18666 (Sigma-Aldrich).[9]

Animals

Mice heterozygous for a spontaneous truncation of the *Npc1* gene, BALB/c Nctr-Npc1m1N/J mice (#003092) were obtained from The Jackson Laboratory (Bar Harbor, USA). Males and females of the two strains were crossed in-house to generate *Npc1*$^{-/-}$ and wild-type littermates (*Npc1*$^{+/+}$). Mice received a normal chow diet and water *ad libitum* and were housed in a temperature and humidity controlled room with a 12h light/dark cycle. National and local ethical committee approval was obtained for conducting animal experiments and laboratory animal welfare rules were enforced (DBC101698 and DBC17AC). In order to anesthetize mice, Hypnorm (0.315 mg/mL phenyl citrate and 10 mg/mL fluanisone) and Dormicum (5 mg/mL midazolam) was administered according to their weight (80 µL per 10g body weight) and subsequent cervical dislocation was performed. Organs were dissected and fixed in 4% formalin for immunohistochemical analysis or snap-freezed for protein and mRNA analysis.

Electron microscopy and toluidine blue staining

For transmission electron microscopy (TEM) and toluidine blue staining, fresh liver was fixed in paraformaldehyde/glutaraldehyde (Karnovsky's fixative) and post-fixed with 1% osmium tetroxide. The fixed tissue samples were block-stained with 1% uranyl acetate, dehydrated in dimethoxypropane, and embedded in epoxyresin LX-112. 0.5 µm-thick sections were stained with toluidine blue and imaged by brightfield microscopy (Leica DM5500B) with an HCX PL APO 63x/1.40-0.60 Oil immersion objective. For TEM, ultrathin sections were stained with tannic acid, uranyl acetate, and lead citrate. Examination was performed using a Philips CM10 transmission electron microscope (Eindhoven, The Netherlands). Images were acquired using a digital transmission EM camera (Morada 10-12, Soft Imaging System, RvC, Soest, The Netherlands).

Immunohistochemistry and immunofluorescence

Dissected tissue was fixed in 4% formalin (pH 7.0 by phosphate buffer), and embedded in paraffin. Embedded tissue was cut in 4 µm-thick sections, washed in 100% xylene to remove paraffin, and washed in 100% ethanol. Rehydration occurred through incubation in 96% ethanol, 70% ethanol and milliQ water respectively and heat induced epitope retrieval (HIER) was performed at 98°C for 10 minutes in 10 mM citric acid (pH 6). Tissues were washed and permeabilized in PBS/0,01% Tween-20 (CAS 9005-64-5, Sigma) and incubated with primary antibodies goat-anti-GPNMB (AF2330; R&D Systems, Abingdon, UK), rat-anti-galectin-3 clone M3/38 (MABT51, Millipore; pre-blocked with 5% mouse serum and centrifuged), rabbit-anti-LAMP1 (ab24170, Abcam) or rabbit-anti-SCARB2 (NB400-129, Novus Biologicals). Antibodies were diluted in PBS/5% antibody diluent (ScyTek Laboratories). In order to prepare immunohistochemistry for spectral imaging,

slides stained for SCARB2 were washed and incubated with alkaline phosphatase-conjugated poly-AP goat anti-rabbit IgG (BrightVision; ImmunoLogic, Klinipath, Duiven, The Netherlands). Bound AP was visualized through incubation with AP substrate VectorBlue (SK-5300; Vector Laboratories, Burlingame, CA, USA) in presence of 0.2 mM levamisole to inhibit endogenous alkaline phosphatase activity. For double staining, slides were washed and subjected to a second HIER to inactivate and remove existing antibody-antigen bonds while leaving the precipitated chromogen unchanged.[31] Sections were incubated with rabbit anti-IBA1 (019-19741, WAKO Chemicals), rat anti-galectin-3 clone M3/38 (MABT51) or rabbit anti-cathepsin D (antiserum was prepared in our laboratory) and subsequently washed, and incubated with poly-AP goat anti-rabbit IgG or goat anti-rat IgG according to their respective primary antibody. Development of signal was performed through incubation with VectorRed AP substrate (SK-5100; Vector Laboratories) in presence of 0.2 mM levamisole. Sections were mounted with VectaMount (Vector Laboratories). Images were obtained by brightfield microscopy (Leica DM5500B) with an HC PLAN APO 20x/0.70 or HCX PL APO 63x/1.40-0.60 Oil objective. Nuance imaging system (Perkin Elmer, Hopkinton, MA, USA) allowed acquisition of multispectral data sets from 420 to 720 nm with 10nm intervals. Single-stained sections were used to define the spectral properties of each colour in order to unmix the double staining patterns. Construction of composite images was done by Nuance 3.0.2 software, which rendered display intensity heat maps for single channels and subsequently allowing a colour universal design. With respect to immunofluorescence analysis, aforementioned primary antibodies were visualized by secondary donkey antibodies against rabbit or goat IgG, conjugated to Alexa Fluor™ 647 (Molecular Probes, A31573 and A21447 resp.). For detection of galectin-3, goat-anti-rat IgG conjugated to TxR was used (Southern Biotech, 3052-07). Images were obtained by fluorescence microscopy (Leica DM5500B) with an HCX PL APO 63x/1.40-0.60 Oil objective.

Enzyme activity assays

Protein quantification of cell and tissue homogenates was assessed by bicinchoninic acid assay (Thermo Fisher Scientific, 23225). Equal protein amounts were used for enzyme activity assays. GCase activity was assayed using 4-methylumbelliferyl (4-MU) substrate beta-D-glucopyranoside (44059, Glycosynth) in McIlvaine buffer, pH 5.2, with 0.1% (w/v) BSA.[32]

Activity-based probe analysis

Where stated, homogenates of tissue and cells were labelled with excess of activity-based probe (ABP) conjugated to a fluorescent dye as earlier described.[33] When GCase was labelled in lysates of cultured cells (Figure 4), ultrasensitive labeling of all active GCase molecules was performed using 100 nM ABP-ME569 (Cy5, in 0.5-1% DMSO).[33] Incubation was performed for 1h at 37°C. In homogenates of tissue (Figure 2), GCase and GBA2 were labelled using a broad specificity ABP for retaining β-exoglucosidases, ABP-JJB367 (containing Cy5).[34] Labelling occurred at 200 nM ABP-JJB367 at pH 5.8 (0,5-1% DMSO) for 1h on ice. Samples were denatured and separated by SDS-PAGE. Detection of fluorescence in wet gel slabs was performed using a Typhoon FLA 9500 fluorescence scanner (GE Healthcare). Far red fluorescence (ME569 and JJB367) was detected using λEX 635 nm and λEM ≥ 665 nm. After imaging, gels were either stained by Coomassie

G250 for total protein and scanned on ChemiDoc MP imager (Bio-Rad) or used for western blotting.[33]

Western Blot Analysis

Frozen tissue samples and cultured cells were lysed in KPi lysis buffer (25 mM K_2HPO_4/KH_2PO_4, pH 6.5, 0.1% [v:v] Triton X-100) supplemented with protease inhibitors (Roche) and sonicated 5x 1 second with 9 minutes interval (amplitude 25%). Equal quantities of protein as assessed by bicinchoninic acid assay (Thermo Fisher Scientific, 23225) were resuspended in Laemmli buffer and denatured at 95°C. Proteins were subsequently separated by SDS-PAGE using a 10% acrylamide gel and transferred to 0,2 µm nitrocellulose membrane (#1704159, Biorad). Blocking of membranes occurred in 5% (w:v) bovine serum albumin (Sigma, A1906) solution in PBS/0.1% Tween-20 (Sigma, P1379) for 1 h at room temperature (RT). Primary antibodies used were targeted against GPNMB (AF2330; R&D Systems), LIMP2 (NB400-129, Novus Biologicals), LAMP1 (ab24170, Abcam) and galectin-3 (MABT51, Millipore). Furthermore, mouse-anti-tubulin (Cedarlane, CLT 9002) was used as loading control. Proteins were detected by using specific secondary conjugated antibodies (Alexa Fluor™ 488/647) (Molecular Probes). Detection of immunoblots was performed using a Typhoon FLA 9500 fluorescence scanner (GE Healthcare).

RNA Extraction and Real-time PCR

Total RNA from liver or cell culture was extracted by means of the NucleoSpin II extraction kit (Macherey Nagel) according to manufacturer's protocol. RNA concentrations were measured (DeNovix DS-1) and equal amounts of RNA were used for cDNA synthesis according to the manufacturer's protocol (Invitrogen). Real time qPCR was performed using Bio-Rad CFX96 Touch™ real-time PCR detection system (Bio-Rad Laboratories). Acidic ribosomal phosphoprotein 36B4 expression (*Rplp0*) was used as reference.

References

1. Infante, R. E., Wang, M. L., Radhakrishnan, A., Hyock, J. K., Brown, M. S. & Goldstein, J. L. NPC2 facilitates bidirectional transfer of cholesterol between NPC1 and lipid bilayers, a step in cholesterol egress from lysosomes. *Proc. Natl. Acad. Sci. USA.* **105**, 15287–15292 (2008).
2. Vanier, M. T. Niemann-Pick disease type C. *Orphanet J. Rare Dis.* **5**, 16 (2010).
3. Elleder, M., Smíd, F., Hyniová, H., Čihula, J., Zeman, J. & Macek, M. Liver findings in Niemann-Pic disease type C. *Histochem. J.* **16**, 1147–1170 (1984).
4. Pentchev, P. G., Gal, A. E., Booth, A. D., Omodeo-Sale, F., Fours, J., Neumeyer, B. A., Quirk, J. M., Dawson, G. & Brady, R. O. A lysosomal storage disorder in mice characterized by a dual deficiency of sphingomyelinase and glucocerebrosidase. *Biochim. Biophys. Acta - Lipids Lipid Metab.* **619**, 669–679 (1980).
5. Vanier, M. T. Biochemical studies in niemann-pick disease I. Major sphingolipids of liver and spleen. *Biochim. Biophys. Acta - Lipids Lipid Metab.* **750**, 178–184 (1983).
6. Salvioli, R., Scarpa, S., Ciaffoni, F., Tatti, M., Ramoni, C., Vanier, M. T. & Vaccaro, A. M. Glucosylceramidase mass and subcellular localization are modulated by cholesterol in Niemann-Pick disease type C. *J. Biol. Chem.* **279**, 17674–17680 (2004).
7. Ferraz, M. J., Marques, A. R. A. A., Gaspar, P., Mirzaian, M., van Roomen, C., Ottenhoff, R., Alfonso, P., Irún, P., Giraldo, P., Wisse, P., Sá Miranda, C., Overkleeft, H. S. & Aerts, J. M. Lyso-glycosphingolipid abnormalities in different murine models of lysosomal storage disorders. *Mol. Genet. Metab.* **117**, 186–93 (2016).
8. Ferraz, M. J., Marques, A. R. A., Appelman, M. D., Verhoek, M., Strijland, A., Mirzaian, M., Scheij, S., Ouairy, C. M., Lahav, D., Wisse, P., Overkleeft, H. S., Boot, R. G. & Aerts, J. M. Lysosomal glycosphingolipid catabolism by acid ceramidase: formation of glycosphingoid bases during deficiency of glycosidases. *FEBS Lett.* **590**, 716–725 (2016).
9. Marques, A. R. A., Mirzaian, M., Akiyama, H., Wisse, P., Ferraz, M. J., *et al.* Glucosylated cholesterol in mammalian cells and tissues: formation and degradation by multiple cellular β-glucosidases. *J. Lipid Res.* **57**, 451–63 (2016).
10. Marques, A. R. A., Aten, J., Ottenhoff, R., van Roomen, C. P. A. A., Herrera Moro, D., Claessen, N., Vinueza Veloz, M. F., Zhou, K., Lin, Z., Mirzaian, M., Boot, R. G., De Zeeuw, C. I., Overkleeft, H. S., Yildiz, Y. & Aerts, J. M. F. G. Reducing GBA2 activity ameliorates neuropathology in Niemann-Pick type C mice. *PLoS One* **10**, e0135889 (2015).
11. Reczek, D., Schwake, M., Schröder, J., Hughes, H., Blanz, J., Jin, X., Brondyk, W., Van Patten, S., Edmunds, T., Saftig, P. LIMP-2 Is a receptor for lysosomal mannose-6-phosphate-independent targeting of β-glucocerebrosidase. *Cell* **131**, 770–783 (2007).
12. Zachos, C., Blanz, J., Saftig, P. & Schwake, M. A critical histidine residue within LIMP-2 mediates pH sensitive binding to its ligand β-glucocerebrosidase. *Traffic* **13**, 1113–1123 (2012).
13. Schwake, M., Schröder, B. & Saftig, P. lysosomal membrane proteins and their central role in physiology. *Traffic* vol. 14 739–748 (2013).
14. Heybrock, S., Kanerva, K., Meng, Y., Ing, C., Liang, A., *et al.* Lysosomal integral membrane protein-2 (LIMP-2/SCARB2) is involved in lysosomal cholesterol export. *Nat. Commun.* **10**, 3521 (2019).
15. Hollak, C. E. M., van Weely, S., van Oers, M. H. J. & Aerts, J. M. F. G. Marked elevation of plasma chitotriosidase activity. A novel hallmark of Gaucher disease. *J. Clin. Invest.* **93**, 1288–1292 (1994).
16. Boot, R. G., Verhoek, M., de Fost, M., Hollak, C. E. M., Maas, M., Bleijlevens, B., van

Breemen, M. J., van Meurs, M., Boven, L. A., Laman, J. D., Moran, M. T., Cox, T. M. & Aerts, J. M. F. G. Marked elevation of the chemokine CCL18/PARC in Gaucher disease: a novel surrogate marker for assessing therapeutic intervention. *Blood* **103**, 33–39 (2004).

17. Ferraz, M. J., Kallemeijn, W. W., Mirzaian, M., Herrera Moro, D., Marques, A., Wisse, P., Boot, R. G., Willems, L. I., Overkleeft, H. S. & Aerts, J. M. Gaucher disease and Fabry disease: new markers and insights in pathophysiology for two distinct glycosphingolipidoses. *Biochim. Biophys. Acta - Mol. Cell Biol. Lipids* **1841**, 811–825 (2014).

18. Kramer, G., Wegdam, W., Donker-Koopman, W., Ottenhoff, R., Gaspar, P., Verhoek, M., Nelson, J., Gabriel, T., Kallemeijn, W., Boot, R. G., Laman, J. D., Vissers, J. P. C., Cox, T., Pavlova, E., Moran, M. T., Aerts, J. M. & van Eijk, M. Elevation of glycoprotein nonmetastatic melanoma protein B in type 1 Gaucher disease patients and mouse models. *FEBS Open Bio.* **6**, 902–913 (2016).

19. Van Der Lienden, M. J. C., Gaspar, P., Boot, R., Aerts, J. M. F. G. & Van Eijk, M. Glycoprotein non-metastatic protein B: an emerging biomarker for lysosomal dysfunction in macrophages. *Int. J. Mol. Sci.* **20** 66 (2019).

20. Aerts, J. M. F. G., Kuo, C. L., Lelieveld, L. T., Boer, D. E. C., van der Lienden, M. J. C., Overkleeft, H. S. & Artola, M. Glycosphingolipids and lysosomal storage disorders as illustrated by Gaucher disease. *Curr. Opin. Chem. Biol.* **53** 204–215 (2019).

21. Guo, Y., He, W., Boer, A. M., Wevers, R. A., de Bruijn, A. M., Groener, J. E. M., Hollak, C. E. M., Aerts, J. M. F. G., Galjaard, H. & van Diggelen, O. P. Elevated plasma chitotriosidase activity in various lysosomal storage disorders. *J. Inherit. Metab. Dis.* **18**, 717–722 (1995).

22. Marques, A. R. A., Gabriel, T. L., Aten, J., Van Roomen, C. P. A. A., Ottenhoff, R., Claessen, N., Alfonso, P., Irún, P., Giraldo, P., Aerts, J. M. F. G. & Van Eijk, M. Gpnmb is a potential marker for the visceral pathology in Niemann-Pick type C disease. *PLoS One* **11**, e0147208 (2016).

23. Overkleeft, H. S., Renkema, G. H., Neele, J., Vianello, P., Hung, I. O., Strijland, A., Van Der Burg, A. M., Koomen, G. J., Pandit, U. K. & Aerts, J. M. F. G. Generation of specific deoxynojirimycin-type inhibitors of the non- lysosomal glucosylceramidase. *J. Biol. Chem.* **273**, 26522–26527 (1998).

24. Abela, G. S., Aziz, K., Vedre, A., Pathak, D. R., Talbott, J. D. & DeJong, J. Effect of cholesterol crystals on plaques and intima in arteries of patients with acute coronary and cerebrovascular syndromes. *Am. J. Cardiol.* **103**, 959–968 (2009).

25. Ioannou, G. N., Landis, C. S., Jin, G., Haigh, W. G., Farrell, G. C., Kuver, R., Lee, S. P. & Savard, C. Cholesterol crystals in hepatocyte lipid droplets are strongly associated with human nonalcoholic steatohepatitis. *Hepatol. Commun.* **3**, 776–791 (2019).

26. Bocan, T. M., Schifani, T. A. & Guyton, J. R. Ultrastructure of the human aortic fibrolipid lesion. Formation of the atherosclerotic lipid-rich core. *Am. J. Pathol.* **123**, 413–24 (1986).

27. Gabriel, T. L., Tol, M. J., Ottenhof, R., van Roomen, C., Aten, J., *et al.* Lysosomal stress in obese adipose tissue macrophages contributes to MITF-dependent Gpnmb induction. *Diabetes* **63**, 3310–3323 (2014).

28. Sakai, J., Duncan, E. A., Rawson, R. B., Hua, X., Brown, M. S. & Goldstein, J. L. Sterol-regulated release of SREBP-2 from cell membranes requires two sequential cleavages, one within a transmembrane segment. *Cell* **85**, 1037–1046 (1996).

29. Gaspar, P., Kallemeijn, W. W., Strijland, A., Scheij, S., Van Eijk, M., Aten, J., Overkleeft, H. S., Balreira, A., Zunke, F., Schwake, M., Sá Miranda, C. & Aerts, J. M. F. G. Action myoclonus-renal failure syndrome: diagnostic applications of activity-based probes and lipid analysis. *J. Lipid Res.* **55**, 138–45 (2014).

30. de Boer, J. F., Kuipers, F. & Groen, A. K. Cholesterol Transport Revisited: A new turbo mechanism to drive cholesterol excretion. *Trends Endocrinol. Metab.* **29** 123–133 (2018).

31. de Boer, O. J., van der Meer, J. J., Teeling, P., van der Loos, C. M., Idu, M. M., van Maldegem, F., Aten, J. & van der Wal, A. C. Differential expression of interleukin-17 family cytokines in intact and complicated human atherosclerotic plaques. *J. Pathol.* **220**, 499–508 (2010).

32. Aerts, J. M. F. G., Donker-Koopman, W. E., Vliet, M. K., Jonsson, L. M. V., Ginns, E. I., Murray, G. J., Barranger, J. A., Tager, J. M. & Schram, A. W. The occurrence of two immunologically distinguishable beta-glucocerebrosidases in human spleen. *Eur. J. Biochem.* **150**, 565–574 (1985).

33. Witte, M. D., Kallemeijn, W. W., Aten, J., Li, K.-Y., Strijland, A., Donker-Koopman, W. E., van den Nieuwendijk, A. M. C. H., Bleijlevens, B., Kramer, G., Florea, B. I., Hooibrink, B., Hollak, C. E. M., Ottenhoff, R., Boot, R. G., van der Marel, G. A., Overkleeft, H. S. & Aerts, J. M. F. G. Ultrasensitive in situ visualization of active glucocerebrosidase molecules. *Nat. Chem. Biol.* **6**, 907–13 (2010).

34. Kallemeijn, W. W., Li, K. Y., Witte, M. D., Marques, A. R. A., Aten, J., *et al.* Novel activity-based probes for broad-spectrum profiling of retaining β-exoglucosidases in situ and in vivo. *Angew. Chemie - Int. Ed.* **51**, 12529–12533 (2012).